Multiple Backscattering and Depolarization from Water Clouds for a Pulsed Lidar System[1]

KUO-NAN LIOU

Goddard Institute for Space Studies, NASA, New York

AND RICHARD M. SCHOTLAND

Dept. of Meteorology and Oceanography, New York University

(Manuscript received 23 November 1970, in revised form 9 March 1971)

ABSTRACT

A computational approach for the multiple backscattering from spherical cloud droplets for a collimated pulsed radar system has been developed, based on the geometry of the system. The radiative transfer relationships include a complete set of Stokes' parameters. The depolarization ratio of the multiple backscattering from a volume of spherically symmetrical and uniformly distributed water drops is obtained.

Calculations are performed for secondary backscattering from water clouds in terms of wavelength, cloud height, beam width and particle number density. It is found that the depolarization does not have a significant dependence on the wavelength in the visible and near visible, or on the distance between the target and receiver. However, the receiver beam width and particle number density significantly affect the depolarization as well as the returned power.

A small receiver beam width, on the order of 10^{-4} rad, is recommended for measurement of the depolarization due to ice crystals in clouds to avoid depolarization caused by multiple scattering from the liquid drops.

1. Introduction

While efforts have been made to investigate the distribution of ice or water in clouds, success has been limited. One of the objectives of a research program initiated at New York University has been to develop a means for distinguishing between ice and water clouds utilizing optical laser radar techniques. It was proposed that a measurement be made of depolarization in the backscattered laser return to separate ice crystals from cloud drops.

The depolarization technique is not new. Several radar meteorologists such as Atlas *et al.* (1953) and Newell *et al.* (1957) have used this technique for identifying nonspherical raindrops and snowflakes. It has been shown that the backscattered radiation from spherically symmetrical and uniform elements such as water drops retains the polarization of the incident energy, while the scattered radiation from nonspherical ice crystals is partially depolarized (see, e.g., Battan, 1959).

However, the return energy from a "volume" of spherically symmetrical and uniformly distributed cloud drops will be partially depolarized due to multiple scattering. In order to investigate the effect of multiple scattering on depolarization in a collimated pulsed radar system, a theoretical study has been undertaken. It is the purpose of this investigation to estimate on a time-dependent basis the depolarization of the higher orders of scattering for spherically symmetrical and uniformly distributed cloud drops with a linearly polarized laser source.

The effects of multiple scattering on the backscattered radar return were first discussed by Herman (1965) assuming a steady-state condition. Time-dependent multiple scattering has been studied by Dell-Imagine (1965) directly, using radiative transfer relationships. Recently, Weinman and Ueyoshi (1969) have calculated the double scattering of a light pulse scattered from a thin turbid medium by adopting the Laplace transform technique which was developed by Bellman *et al.* (1964) for time-dependent transfer problems. Polarization is not considered in either case.

Since the duration of the light pulse considered in this research is on the order of nanoseconds, it is a time-dependent transfer problem. An approach has been developed, based on the physical geometry with a time restriction, to evaluate the returned power and depolarization of the secondary backscattered radiation in a collimated pulsed radar system for a polarized laser source. A generalized time-dependent multiple scattering model for this problem is presented separately by Liou (1971). It is shown that the returned power and depolarization due to photons scattered more than twice is insignificant in most collimated systems.

The cloud particle size distribution chosen for generating the Mie phase functions (scattering diagrams) in this study is the cloud model used and discussed by

[1] This paper is based on portions of a dissertation submitted by the senior author to New York University in partial fulfillment of the requirements for the degree of Doctor of Philosophy.

Deirmendjian (1964, 1969). This cloud model or a linear combination of two such cloud models reproduces fairly well some of the observed distributions such as those found in cumulus and stratiform clouds typical of meteorological conditions in the atmosphere.

2. Phase function and cloud particle size distribution

The phase function (scattering diagram) may be physically described as a quantity which indicates the angular distribution of energy from a scattering element. The phase function for a complete set of Stokes' parameters is a four by four matrix. If no assumptions are made at all for the scattering medium, the phase matrix contains 16 independent coefficients. However, as shown by Perrin (1942) and van de Hulst (1957, Chap. 5), if a sample of particles is randomly oriented and has a plane of symmetry, then the number of independent coefficients is reduced to six. Furthermore, for particles having spherical symmetry, the number of independent coefficients is further reduced to four. Thus, the phase function for a polydispersion of spherical particles can be written as

$$\frac{P_j(\theta)}{4\pi}=\frac{1}{\beta_s k^2}\int_{r_1}^{r_2} i_j(\theta)\frac{dn(r)}{dr}dr, \quad j=1,2,3,4, \qquad (1)$$

where $P_j(\theta)$ and $i_j(\theta)$ are dimensionless quantities [the

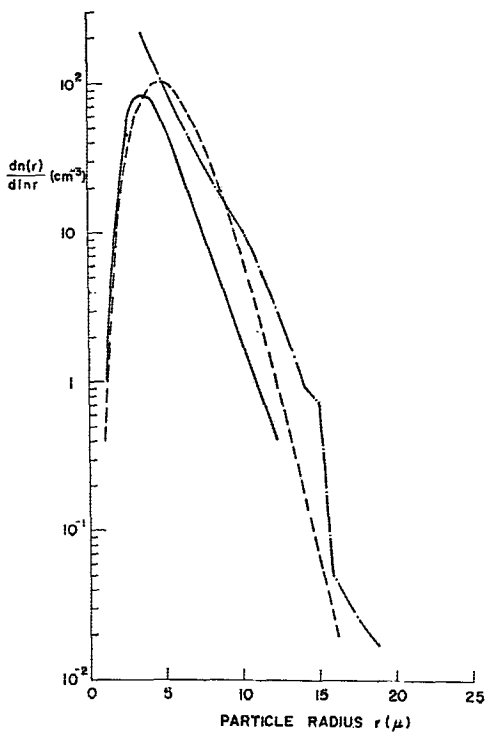

FIG. 1. Comparison of the cloud model with mode radius at 4μ to the observed size distribution of fair weather cumulus: solid line, Diem (1948) fair weather cumulus; dash-dotted line, Battan and Reitan (1957) 19 fair weather cumulus [$\bar{N}=293$ cm^{-3}]; dashed line, cloud model C4[$N=100$ cm^{-3}].

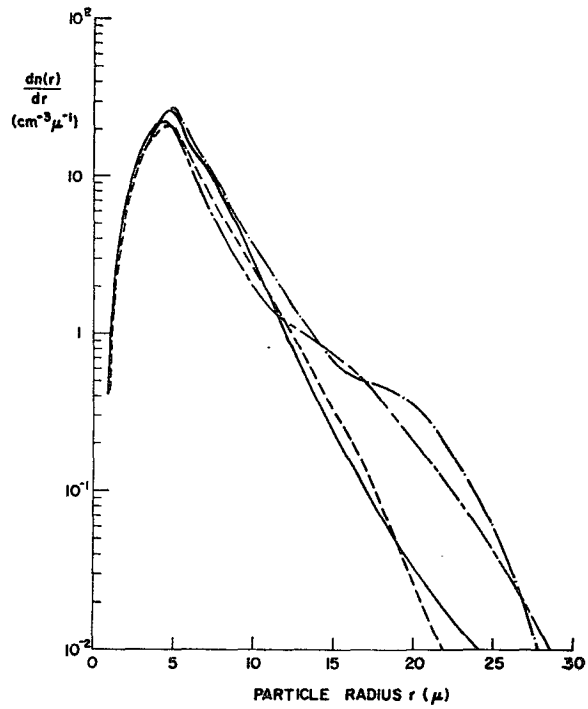

FIG. 2. Comparison of the bimodal distributions to the observed size distributions of cumulus and layered clouds: solid line, Durbin (1959), cumulus type I, thickness 230–2100 m; dash-dotted line, Singleton and Smith (1960), layer cloud, thickness 210–230 m; dash-dashed line and dashed lines, bimodal distributions, with $r_c=4$, $7\,\mu$ and 4, $10\,\mu$, respectively, and $\bar{N}=100$ cm^{-3}.

$i_j(\theta)$ numbers being defined in the usual manner for a single particle (see, e.g., Diermendjian, 1961)], θ is the scattering angle, k the wavenumber, r_1 and r_2 the lower and upper limits of particle radius, respectively,

$$\beta_s=\int_{r_1}^{r_2}\sigma_s\frac{dn(r)}{dr}dr=\bar{\sigma}_s N, \qquad (2)$$

where β_s (length^{-1}) represents the volume scattering cross section, σ_s the scattering cross section for a single particle, $\bar{\sigma}_s$ the averaged value with respect to the particle size distribution, and N the total number of particles per unit volume, which for a homogeneous cloud is a constant. The assumption is made that the particle size distribution is the same throughout the cloud.

The particle size distribution, $dn(r)/dr$, chosen in generating the phase functions is the cloud model or "modified gamma" distribution suggested by Deirmendjian (1964). This size distribution function is a generalization of that first proposed by Borovikov *et al.* (1961) for clouds and can be written as

$$\frac{dn(r)}{dr}=N\frac{6^6}{5!}\frac{1}{r_c}\left(\frac{r}{r_c}\right)^6 e^{-6r/r_c}, \qquad (3)$$

where $dn(r)/dr$ represents the number of particles per micron interval at size r, and r_c is the mode radius at which the concentration is at a maximum.

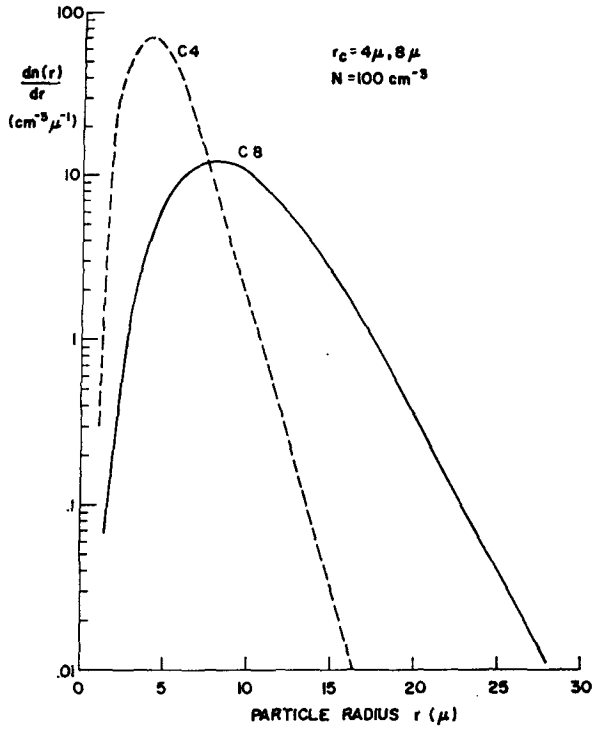

FIG. 3. Two cloud models with mode radii at 4 and 8μ.

The cloud model with $r_c=4\,\mu$, and $N=100$ cm^{-3} describes some of the averaged observed spectra for fair weather cumulus reported by Diem (1948) and Battan and Reitan (1957), shown in Fig. 1. As indicated, the size distribution for at least some fair weather cumulus is very narrow and drops off very rapidly, with the number of particles in the tail being negligible.

However, the observed size distributions for clouds normally contain more droplets in the tail region than is predicted by the modified gamma distribution. A linear combination of two modified gamma distributions was used to fit some of the observed size distributions. As shown in Fig. 2, the composite distribution with two mode radii at 4 and 7 μ fits the observed distribution of the cumulus type 1 reported by Durbin (1959), while mode radii at 4 and 10 μ fit the observed distribution of the layered cloud with thickness from 210–300 m reported by Singleton and Smith (1960). The particle number density used for the cloud models in Fig. 2 is also 100 cm^{-3}. It should be noted that in Fig. 2 the verticle axis is dn/dr [cm^{-3} μ^{-1}], while in Fig. 1 it is $dn/d\ln r$ [cm^{-3}]. The size distributions of the cumulus congestus, cumulonimbus and tropical cumulus observed by Weickmann and aufm Kampe (1953), Diem, and Battan and Reitan are very broad. The mean radii for these distributions have a range from about 7–9 μ which approximately corresponds to the modified gamma distribution with mode radius at 8 μ. Fig. 3 shows the size distributions for two cloud models with mode radii at 4 and 8 μ. It is seen that the cloud model for $r_c=8\,\mu$ denotes the size distribution for large particles compared to that for $r_c=4\,\mu$.

The particle concentration and water content of layered and convective clouds reported by Singleton and Smith (1960) and Squires (1957) vary from about 50–500 cm^{-3} and about 0.1–3 gm m^{-3}, respectively, for different layers in the cloud. The cloud droplets are not homogeneously distributed in the horizontal or vertical directions. Our knowledge of the spatial variation of the drop size distribution is still quite limited. We have assumed for the purposes of the scattering computation that the cloud droplet parameters are uniform through the cloud.

We have made computations[2] to examine how sensitive the resulting phase functions are to the large particle cutoff of the size distributions. For mode radii $r_c=4$ and 8 μ, with wavelength 0.6943 μ, the ranges of the size distribution have been selected to be 0–17 μ and 0–30 μ. Little difference is found between the results of computations of these two ranges for two mode radii. Thus, it appears that these phase functions are not too sensitive to the cutoff in the tail of the size distribution. It is felt that the reason for this is that the size distribution drops very rapidly, so that not many larger particles remain in the tail. The phase functions were also

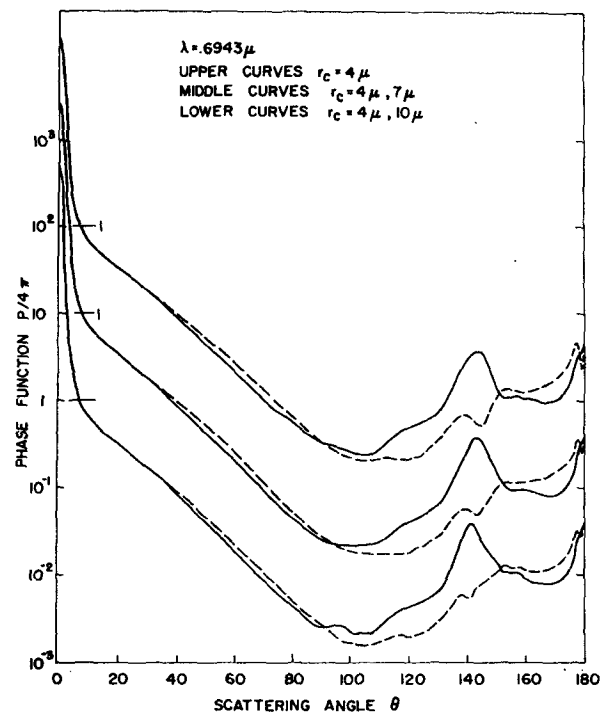

FIG. 4. Single-scattering phase functions perpendicular (solid lines) and parallel (dotted lines) to the scattering plane for water drops illuminated by 0.6943 μ radiation. In Figs. 4–6 the vertical scales apply to the lowermost curve, while the scales for the other curves may be obtained by multiplication by a power of 10 such that the horizontal bar on each curve occurs at unity.

[2] The Mie scattering program was kindly supplied by Dr. J. Hansen at the Institute for Space Studies.

TABLE 1. Index of refraction and mean scattering cross section for water clouds.

λ (μ)	n_r	n_i	C4(0–17μ) $\bar{\sigma}_s$ (10^{-8} m^2)	C8(0–24μ) $\bar{\sigma}_s$ (10^{-8} m^2)
0.3472	1.349	8×10^{-9}	0.01637	0.06394
0.6943	1.330	3.3×10^{-8}	0.01682	0.06551
1.06	1.325	1.07×10^{-6}	0.01721	0.06606

Note: The single-scattering albedo $\tilde{\omega}_0$ is nearly unity ($\geqslant 0.999$) for all cases.

computed for two composite distributions. One has modes at 4 and 7 μ, a model corresponding to Durbin's cumulus type 1, and the other one has modes at 4 and 10 μ which is similar to one of the layer clouds reported by Singleton and Smith. Fig. 4 shows the phase functions for the two composite distributions at a wavelength of 0.6943 μ. When these are compared in Fig. 4 to the phase functions for a gamma distribution with $r_c=4\,\mu$, in general no considerable change is found.

The analysis of the effects of size distribution on the scattering computations is quite complicated. It is felt that at least two parameters for the size distribution have to be considered, i.e., the mean size and the dispersion. While more detailed studies are required for the purpose of estimating the returned power and depolarization of multiple backscattering in this study, we

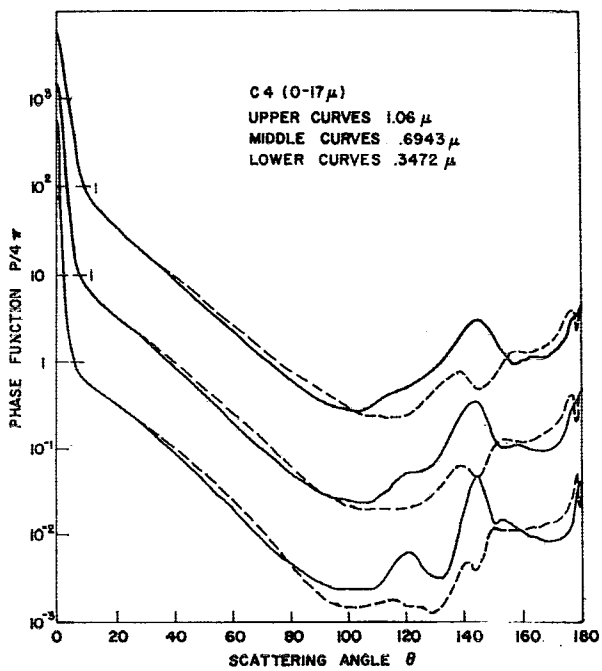

FIG. 5. Single-scattering phase functions perpendicular (solid lines) and parallel (dotted lines) to the scattering plane for water drops illuminated by 1.06 μ (upper curves), 0.6943 μ (middle curves), and by 0.3472 μ (lower curves). The size distribution has the mode radius at 4 μ.

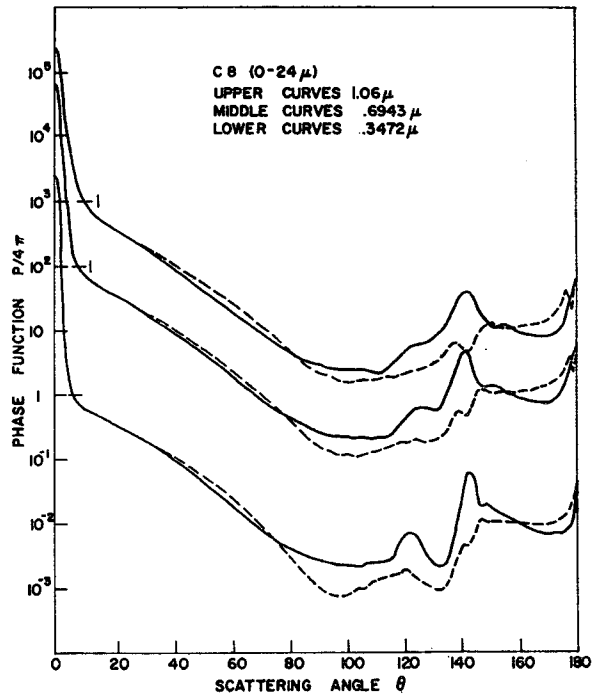

FIG. 6. Same as in Fig. 5 except for a mode radius at 8 μ.

choose $r_c=4\,\mu$ to represent the less dense clouds such as fair weather cumulus, while $r_c=8\,\mu$ represents larger and denser clouds such as cumulus congestus and cumulonimbus. The cloud models for $r_c=4$ and 8 μ are denoted as C4 and C8, respectively, for simplicity. Three typical laser wavelengths [0.6943 μ (ruby), 1.06 μ (neodumium) and 0.3472 μ (doubled ruby)] are used in generating the phase functions for two clouds for $r_c=4$ and 8 μ. For the index of refraction of water drops at each wavelength, we have used the summary data published by Irvine and Pollack (1968). As shown in Table 1, the imaginary part n_i of the index refraction is negligibly small compared to the real part n_r for wavelengths in the visible and near visible. The single scattering albedo ($\geqslant 0.999$) is nearly unity for all three wavelengths, and the mean scattering and extinction cross sections are approximately equal. Hence, the absorption in the water clouds may be ignored, so that in those spectral regions water clouds may be considered as non-absorptive medium.

Figs. 5 and 6 show the phase functions for C4 and C8 respectively, for three different wavelengths. For a fixed cloud model, the rainbow, the glory, and the forward diffraction peak due to single scattering become less pronounced for longer incident wavelengths. Moreover, the features for C8 are more pronounced than those of C4. These features can be examined in terms of the nondimensional parameter, the ratio of the circumference of a drop to the incident wavelength.

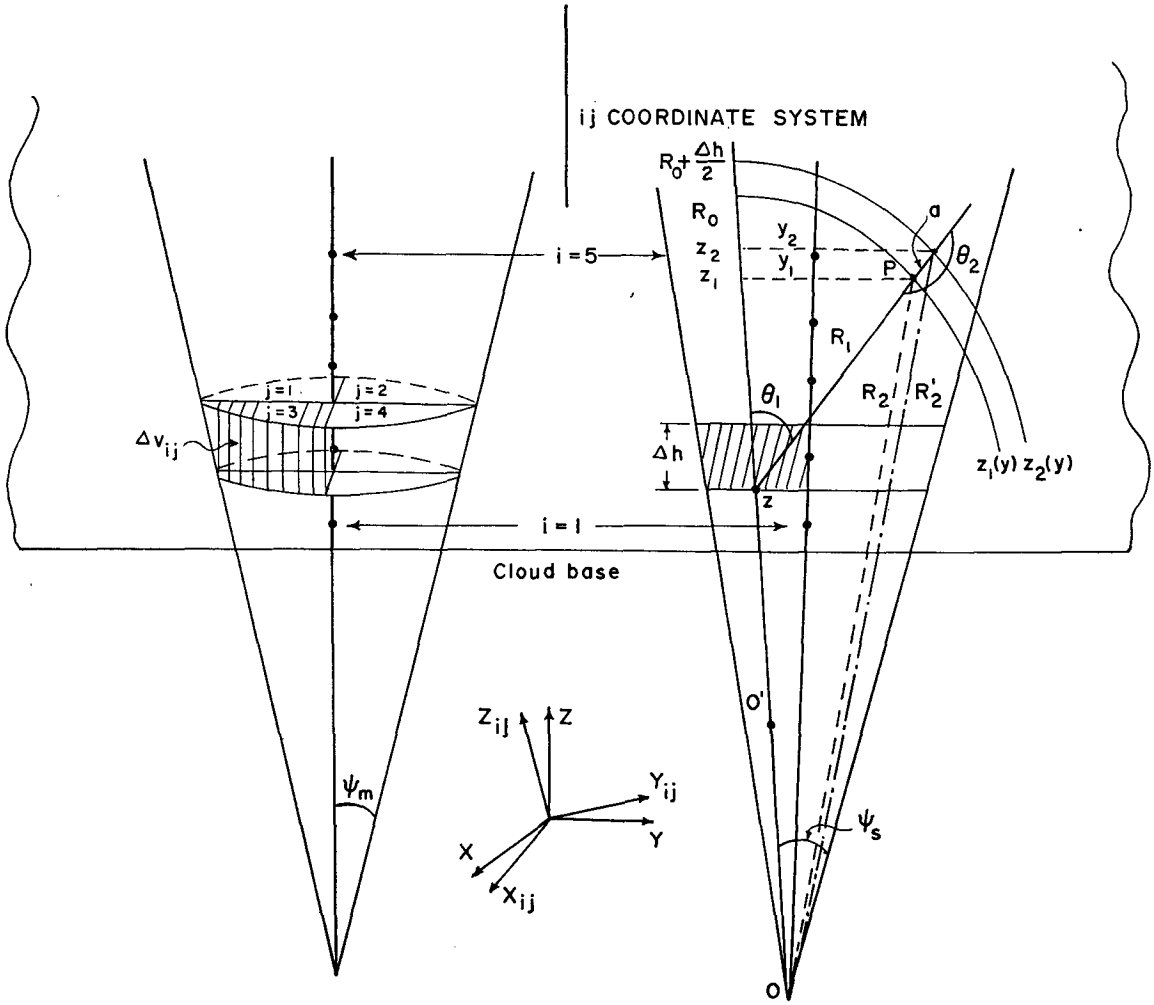

FIG. 7. The left-hand side represents a three-dimensional outgoing pulse which is divided into four sub-pulses in the horizontal plane for simplicity of illustration. The number of sub-pulses is denoted as j, while the black dots along the z direction inside the cloud represent the number of pulses i. The right-hand side is a two-dimensional diagram for the secondary backscattering. The transmitter and receiver cone are assumed to be the same in this figure. The line 00′ is the vertical direction in the ij coordinate system (i.e., z_{ij}). The lower central figure represents the coordinate system of the receiver. All symbols are explained in the text.

3. Physical system

In a collimated pulsed light system, the transmitter and receiver are coaxial. The transmitter sends out a linearly polarized pulse of energy for a period on the order of nanoseconds. One measures, in general, all orders of backscattering at a given instant of time in addition to the primary backscattering. In order for the primary and secondary backscattered radiation to reach the receiver at a given instant in time, there must exist a geometric relationship between R_0, R_1, and R_2 (as indicated in Fig. 7) such that

$$\frac{2R_0}{c}=\frac{z+R_1+R_2}{c}=t_3, \tag{4}$$

i.e.,

$$R_1+R_2=2R_0-z,$$

where R_0 is the distance at which the scattering occurs for the primary backscattering. For the secondary backscattering, $z(x,y)$ is the height at which the first scattering occurs at the point (x,y) in the horizontal plane, R_1 the distance from the first scattering to the second scattering, R_2 the distance from the second scattering to the receiver, and c the velocity of light.

Schotland *et al.* (1965) have indicated that (4) essentially corresponds to a trace of ellipses with two foci at points 0 and z. Referring to Fig. 7 we divide the pulse into several sub-pulses, the base of the pulse passing through the "fixed positions" z, P at times t_1 and t_2, respectively, and returning to the receiver at time t_3. Meanwhile, some of the light will have been scattered from the top of the pulse, as it passes the fixed positions at times $(t_1-\Delta h/c)$, $(t_2-\Delta h/c)$. In order for all the secondary backscattered light of a sub-pulse to return

to the receiver at a given instant of time, the following condition must be satisfied:

$$\frac{1}{c}(R_2'-R_2+a)=\frac{\Delta h}{c}, \tag{5}$$

where R_2' and a are quantities which can be calculated in terms of the variables y, z, R_0 and R_1 by means of geometrical relationships, together with (4) and (5). For given R_0, x, y, and z, (R_1+R_2) is constant with respect to the base of the pulse. On the other hand, $(R_1+a+R_2')=(R_1+R_2+\Delta h)$ is constant with respect to the top of the pulse. Hence, they correspond to two confocal ellipses with foci at 0 and z. The separation of the confocal ellipses is approximately $\Delta h/2$. If we define $0'$ as the center of the ellipse, then the corresponding volume for secondary backscattered radiation which will return to the receiver at the same time as the primary backscattering is a shell bounded by these two confocal ellipsoids with a complete revolution with respect to the $00'$ axis.

Let us refer to Fig. 7. For the inner ellipse, the major axis a_1 and minor axis b_1 are

$$\left.\begin{aligned} a_1&=R_0-\frac{z}{2}\\ b_1&=[a_1^2-(z/2)^2]^{\frac{1}{2}}\end{aligned}\right\}, \tag{6}$$

while the corresponding axes for the outer ellipse are

$$\left.\begin{aligned} a_2&=\left(R_0+\frac{\Delta h}{2}\right)-\frac{z}{2}\\ b_2&=[a_2^2-(z/2)^2]^{\frac{1}{2}}\end{aligned}\right\}. \tag{7}$$

The two ellipses with respect to the coordinate axes with origin at 0 can be represented as

$$\frac{y_k^2}{b_k}\ \alpha\frac{\left(z_k-\frac{z}{2}\right)^2}{a_k}=1,\quad k=1,2. \tag{8}$$

To obtain the volume corresponding to secondary backscattering in the pulsed light system, we first evaluate the area between the two ellipses. A small receiver beam width $2\Psi_m$ is assumed so that the maximum receiver half-beam width Ψ_S for each pre-divided sub-pulse may be evaluated from the geometry. Let (Y_{1m},z_{1m}) and (y_{2m},z_{2m}) represent the values for the points (y_1,z_1) and (y_2,z_2), respectively, on the edge of the receiver cone, where the secondary backscattering is limited. Then we have the relationships

$$y_{km}\approx\Psi_S z_{km},\quad k=1,\ 2. \tag{9}$$

We substitute (9) into (8) to determine the values of y_{1m} and y_{2m}. The area bounded by two confocal ellipses may be obtained by integrating the following boundaries in the Y, Z coordinate system:

$$\left.\begin{aligned} y_l&=0\\ y_u&=(y_{1m}+y_{2m})/2\\ z_l&=\frac{z}{2}+a_1\left(1-\frac{y^2}{b_1}\right)^{\frac{1}{2}}\\ z_u&=\frac{z}{2}+a_2\left(1-\frac{y^2}{b_2}\right)^{\frac{1}{2}}\end{aligned}\right\}, \tag{10}$$

where the values (y_l,z_l) and (y_u,z_u) represent the lower and the upper limits in the y and z directions, respectively. It is seen that the integration over the shell has variable boundaries in the z direction. Since the infinitesimal volume bounded by the two confocal ellipsoids can be denoted as $dV=yd\phi dydz$, where ϕ is the azimuth angle, we can then integrate over a complete revolution in ϕ. The volume formed by the two confocal ellipsoids may therefore be evaluated. It should be noted that the scattering distances R_1, R_2 and scattering angles θ_1, θ_2 can be evaluated in terms of the values of y and z by the geometry indicated in Fig. 7.

4. Formulation

To formulate the total secondary backscattered flux density, we divide the outgoing pulse into several sub-pulses from geometry. The volumes of the pre-divided sub-pulses are denoted as Δv_{ij}, and the coordinate system for each ij sub-pulse is named ij coordinate, where i represents the number of sub-pulses in the vertical direction and j the number in the horizontal plane. The flux density due to the first-order scattering at the i position for an element volume of sub-pulse Δv_{ij} may be evaluated as

$$\begin{aligned}\mathbf{F}^{(1)}&=\sum_j\int_{\Delta v_{ij}}\frac{\beta_s}{R_1^2}\mathbf{P}(\theta_1)\mathbf{L}(\phi_1)\mathbf{F}^{(0)}\exp(-\tau_1)d(\Delta v_{ij})\\ &\approx\sum_j\Delta v_{ij}\beta_s\frac{1}{R_1^2}\mathbf{P}(\theta_1)\mathbf{L}(\phi_1)\mathbf{F}^{(0)}\exp(-\tau_1),\end{aligned} \tag{11}$$

where

$$\mathbf{F}^{(0)}=\begin{bmatrix}F_l^{(0)}\\ F_r^{(0)}\\ U^{(0)}\\ V^{(0)}\end{bmatrix},$$

$$\mathbf{P}(\theta)=\begin{bmatrix}P_2(\theta) & 0 & 0 & 0\\ 0 & P_1(\theta) & 0 & 0\\ 0 & 0 & P_3(\theta) & -P_4(\theta)\\ 0 & 0 & P_4(\theta) & P_3(\theta)\end{bmatrix},$$

$$\mathbf{L}(\phi)=\begin{bmatrix}\cos^2\phi & \sin^2\phi & \frac{1}{2}\sin2\phi & 0\\ \sin^2\phi & \cos^2\phi & -\frac{1}{2}\sin2\phi & 0\\ -\sin2\phi & \sin2\phi & \cos2\phi & 0\\ 0 & 0 & 0 & 1\end{bmatrix}.$$

In the above $\mathbf{F}^{(0)}$ is the outgoing flux matrix at the point of first scatter; $\mathbf{P}(\theta)$ represents the four by four phase matrix for a volume of spherically symmetrical scatterers, where each phase element was defined in Section 2; $\mathbf{L}(\phi)$ is the coordinate transformation defined by Chandrasekhar (1960, p. 35) for a complete set of Stokes' parameters. The remaining parameters are the azimuth angle ϕ and the nondimensional optical thickness τ_i for the path R_1.

Let V_{ij} be the volume formed by the revolution of the two elliptic traces with respect to the ij coordinate system. The mean flux density due to the secondary radiation returned to the collecting aperture at the same instant of time as the primary backscattering can be expressed as

$$\mathbf{F}^{(2)}=\sum_i \int_{V_{ij}} \frac{\beta_s}{R_2^2}\mathbf{P}(\theta_2)\mathbf{F}^{(1)} \exp(-\tau_{2p})dV, \quad (12)$$

where τ_{2p} is the optical thickness for the backscattering path R_{2p} inside the cloud. It can be evaluated by using the simple sine law. For a co-axial transmitter and receiver system, the secondary backscatter is in the same scattering plane as the first scattering, so that the rotation of coordinates is not necessary. The summation over i in (11) sums all the possible pulses which can contribute secondary scattering along the vertical direction, while summation over j in (12) sums over each sub-pulse element in each i position. Thus, by substituting (11) into (12), we have

$$\mathbf{F}^{(2)}=\sum_i \sum_j \Delta v_{ij}\beta_s^2 \int_{V_{ij}} \frac{1}{R_1^2R_2^2}\mathbf{P}(\theta_2)\mathbf{P}(\theta_1)\mathbf{L}(\phi_1)\mathbf{F}^{(0)} \times\exp[-(\tau_1+\tau_{2p})]dV. \quad (13)$$

Since $dV=yd\phi_1dydz$, and the initial outgoing radiation is assumed to be independent of the azimuth angle, as a result of integration over a complete revolution, the $\cos^2\phi_1$ and $\sin^2\phi_1$ terms will equal π, while the $\sin 2\phi_1$ and $\cos 2\phi_1$ components appearing in the coordinate transformation will vanish. Thus,

$$\mathbf{F}^{(2)}=\sum_i \sum_j \pi\Delta v_{ij}\beta_s^2 \int_{yl}^{yu} \int_{zl}^{zu} \frac{1}{R_1^2R_2^2} \times \begin{pmatrix} P_2(\theta_2)P_2(\theta_1)[F_l^{(0)}+F_r^{(0)}] \\ P_1(\theta_2)P_1(\theta_1)[F_l^{(0)}+F_r^{(0)}] \\ -2[P_3(\theta_2)P_4(\theta_1)+P_4(\theta_2)P_3(\theta_1)]V^{(0)} \\ 2[P_3(\theta_2)P_3(\theta_1)-P_4(\theta_2)P_4(\theta_1)]V^{(0)} \end{pmatrix} \times\exp[-(\tau_1+\tau_{2p})]ydzdy, \quad (14)$$

where (y_l,z_l) and (y_u,z_u) represent the values for each ij sub-pulse, and the sub-index ij is neglected for simplicity.

For a vertically polarized outgoing radiation $F_l^{(0)}=V^{(0)}=0$, and we may let $F_r^{(0)}=F_{ij}^{(0)}$. Furthermore, in order for the results to be useful in the remote radar problems, we would like to express (14) in the form of a power transfer function. By integrating the Poynting vector over the perpendicular aperture, we found

$$\mathbf{T}^{(2)}=\frac{\mathbf{P}_R^{(2)}}{P_T}=A_p\sum_i \sum_j \pi\left(\frac{P_{ij}^{(0)}}{P_T}\right)\exp(-\tau_0)\Delta h\beta_s^2 \times\int_{yl}^{yu}\int_{zl}^{zu}\frac{1}{R_1^2R_2^2}\begin{pmatrix} P_2(\theta_2)P_2(\theta_1) \\ P_1(\theta_2)P_1(\theta_1) \\ 0 \\ 0 \end{pmatrix} \times\exp[-(\tau_1+\tau_{2p})]ydzdy. \quad (15)$$

It should be noted that $P_{ij}^{(0)}=F_{ij}^{(0)}A_{ij}g_{ij}$, A_{ij} and g_{ij} being the cross-section area and the weighting function of the transmitted power for each ij sub-pulse. The weighting function is assumed to have Gaussian distribution. $\mathbf{T}^{(2)}$ represents the power transfer function for the secondary backscattered radiation. The double summation sums over all possible energy which is scattered by each ij sub-pulse for an outgoing beam, each sub-pulse being considered as a point source. The factor π is due to the integration over a complete revolution. Other symbols in (15) are as follows: $P_{ij}^{(0)}/P_T$ represents the portion of the power without attenuation in each sub-pulse; $\exp(-\tau_0)$ is the attenuation factor up to position i; and Δh is the vertical length of the pulse in which the top of the pulse and the base of the pulse will be scattered twice and returned back to the receiver simultaneously. The square of the volume scattering cross section (β_s^2) demonstrates that the scattering events have occurred twice. Finally, $1/R_1^2$ and $1/R_2^2$ represent the solid angle of a unit area which receives the first scattering and secondary backscattering, respectively.

The phase matrix in (15) represents two components of linear polarization, namely, perpendicular and parallel to the scattering plane. It can be shown that those two components may be considered as approximately in the x and y directions for a small beam width as a result of mapping the scattered Poynting vector on the receiver coordinate. It is seen that for a linearly polarized beam in a preferred plane the depolarization from secondary backscattering will be due to those two components which essentially arise from the coordinate transformation.

The depolarization ratio for the secondary backscattered radiation, assuming a vertically polarized outgoing beam, may be defined as

$$\Delta_v^{(2)}=\frac{P_y^{(2)}}{P_x^{(1)}+P_x^{(2)}}, \quad (16)$$

where $P_x^{(1)}$ is the power received due to primary backscattering which retains the polarization of the incident energy (it can be calculated from the radar equation presented elsewhere), while $P_x^{(2)}$ and $P_y^{(2)}$ are the power received on the vertical and horizontal apertures caused by the secondary backscattering, respectively. The vertical aperture transmits the incident beam.

Similarly, the depolarization ratio for a horizontally polarized outgoing beam is defined as

$$\Delta_h^{(2)} = \frac{P_x^{(2)}}{P_y^{(1)} + P_y^{(2)}}. \tag{17}$$

5. Discussion of results

In the numerical computations, we have assumed that 80% of the total energy is contained within the transmitted beam width. The effect of side lobes is neglected. Moreover, a vertically polarized outgoing beam is assumed in the calculations.

For a beam width on the order of 10^{-2}–10^{-3} rad, the computation shows that the predominant mode of double scattering in this model consists of forward scattering coupled with backward scattering. This is expected because the scattering from clouds due to wavelengths in the visible and near visible is strongly anisotropic with a sharp forward diffraction peak of the phase function at least three or four orders of magnitude larger than the value of the phase function at any other angle.

The phase function near 180° is very sensitive to depolarization. Therefore, for the purpose of this problem, detailed information on the phase function in the forward and backward directions is required. The secondary scattering calculation indicates that the predominant scattering is from 0–2°, and scattering back with an angle of 178–180° (the elevation angle is so small that it may be taken to be zero). The effect of the secondary scattering computations for other angles is found to be at least one order of magnitude smaller than those of the two regions indicated above.

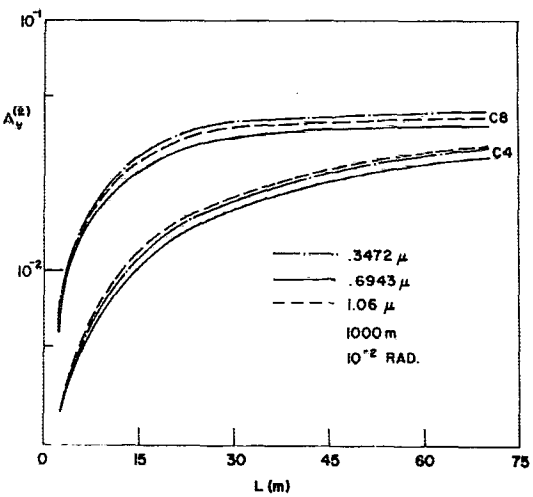

FIG. 8. The resulting value of the second-order depolarization ratio as a function of distance L (in meters) above the cloud base H for three different wavelengths: 0.3472, 0.6943 and 1.06 μ. The upper and lower curves are for cloud models with mode radii at 8 and 4 μ, respectively. The beam width is 10^{-2} rad, the cloud height 1000 m, and the number density 100 cm^{-3}.

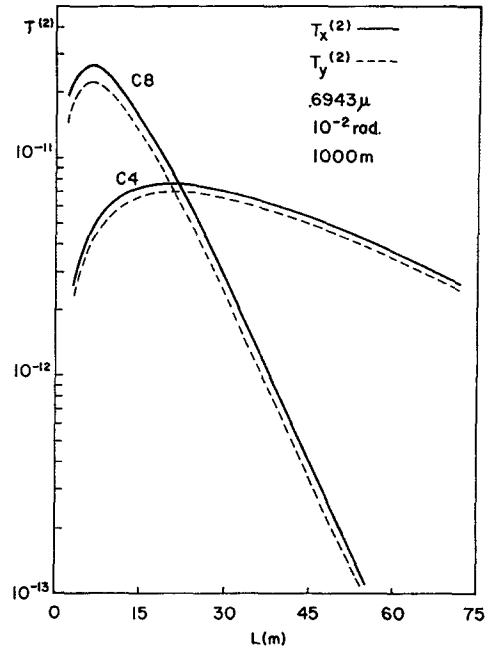

FIG. 9. The second-order power transfer functions $T^{(22)}$ for two cloud models with mode radii at 4 and 8 μ. The solid and dotted lines represent the vertical and horizontal components of second-order power transfer functions, respectively. The particle number density is 100 cm^{-3}.

For convenience in discussing the wavelength dependence of secondary backscattered radiation, we assume a cloud height of 1000 m, a beam width of 10^{-2} rad, and a particle number density of 100 cm^{-3}. No significant differences in the values of $T^{(2)}$ and $\Delta_v^{(2)}$ are found in the calculations for the three wavelengths 0.3472 μ, 0.6943 μ and 1.06 μ in both cloud models. This is because the phase functions and scattering cross sections are similar in the visible and near visible wavelengths for a given cloud model. For the values assumed above, 1–3% of depolarization is found for C4, while 2–4% is seen for that of C8. These are shown in Fig. 8. The depolarization curves seem to approach a limiting value because the return of the primary and secondary scattered energy are both dominated by the exponential attenuation. It should be noted from Figs. 8–14 that the horizontal scale is the distance L (in meters) above the cloud base H. The return time will be $2(H+L)/c$, c being the velocity of light.

From the above, it is known that the second-order transfer function and the depolarization ratio are essentially independent of the wavelength in the visible and near visible. Therefore, for simplicity, we choose ruby

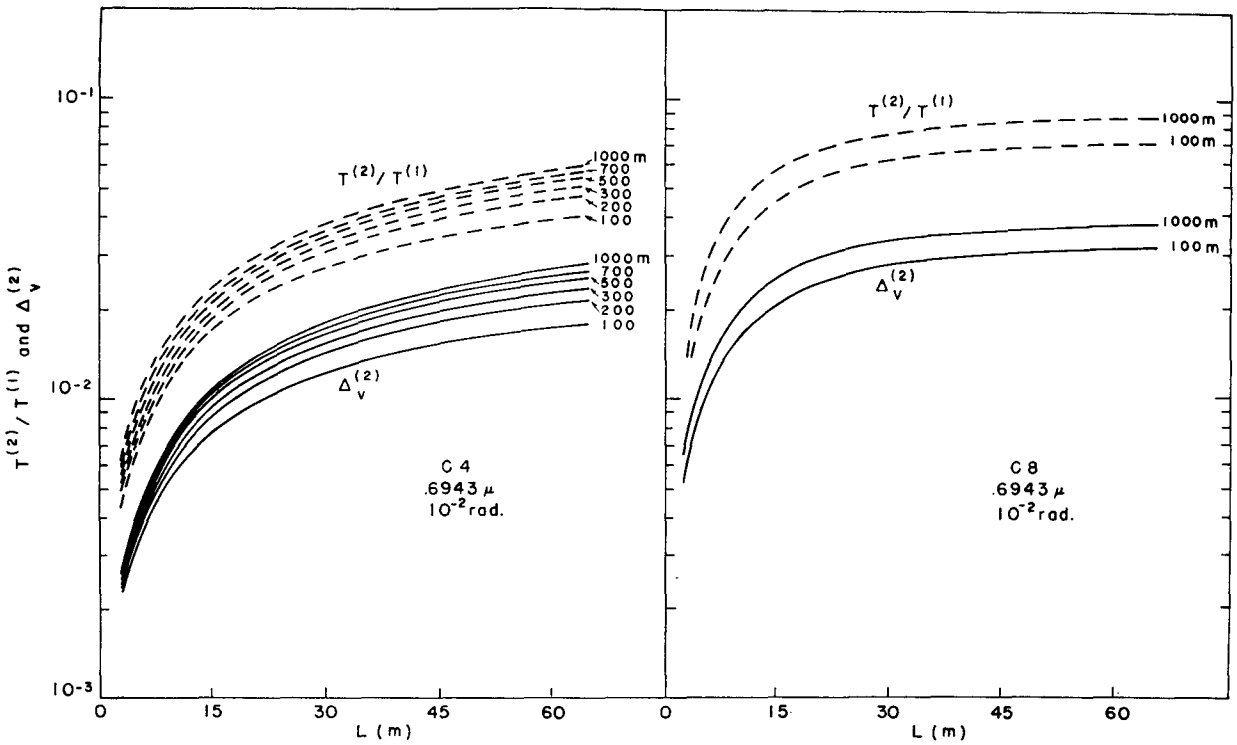

FIG. 10. The ratio of the second- to first-order power transfer functions (dotted lines) and depolarization ratios (solid lines) for two cloud models, C4 (left) and C8 (right), illuminated by 0.6943 μ radiation for different cloud heights. The receiver beam width and particle number density are 10^{-2} rad and 100 cm^{-3}, respectively.

laser light at 0.6943 μ wavelength to perform other physical calculations.

The power received on the collecting aperture depends upon the scattering distances R_1 and R_2. Thus, we would expect that the second-order transfer function varies with the cloud height, which actually is the distance between the receiver and the edge of the target. Fig. 9 shows the comparison of the returned power for two cloud models. Assuming a beam width 10^{-2} rad, and cloud model C4, it is found that the maximum return power occurs approximately at a distance 18 m above the cloud height L, which corresponds to an optical thickness of 0.3. The return power then decreases with increasing L, since the attenuation term begins to dominate the return. For cloud model C8, the maximum return power appears approximately at $L=6$ m, which corresponds to an optical thickness of 0.4. The return energy decreases very rapidly as a result of attenuation, due to the presence of larger particles, where the same particle number density as C4 is assumed. Thus, the incident beam cannot penetrate cloud C8 very far.

The depolarization ratio for different cloud heights is computed for C4 and C8, and is shown in Fig. 10. We find that the change of depolarization with cloud height is quite small, the difference for cloud heights of 100 and 1000 m being only $\sim$0.5%. Since the primary and secondary backscattering both depend upon cloud height, the effect of cloud height on depolarization and on the ratio of the second-order transfer function to the first-order transfer function seems to cancel out. However, because the volume involved for higher clouds is larger for the same width beam than for lower clouds, more multiple scattering would be expected. It appears likely that the depolarization curves for C8 are similar to step functions. From this theoretical calculation, we should expect more depolarization from clouds containing larger drops, if the same particle number density is assumed.

For a given height, the volume contained in a cloud will depend on the receiver beam width. If the beam width is wider, more backscattered energy due to multiple scattering would be expected. It should be noted here that the primary backscattering does not depend upon the geometric cross-sectional area. If the cloud height is 1000 m, as shown in the upper part of Fig. 11, the return power is very sensitive to the beam width for C4 and less sensitive for C8. The distance L for maximum energy return increases with increasing beam width. Beam widths of 10^{-4}, 5×10^{-3}, 10^{-3} and 10^{-2} rad are employed in the calculations. As for depolarizations shown in the lower part of Fig. 11, in cloud C4 a difference of 2% is found between beam widths of 10^{-2} and 10^{-3} rad, and a 1% difference between 10^{-3} and 10^{-4} rad. The depolarization is larger for C8 than for C4, with values of 0.8% for 10^{-4} rad, 3.5% for 10^{-2} rad, and 2–3% for 10^{-3} rad. It is seen that about 4% difference occurs

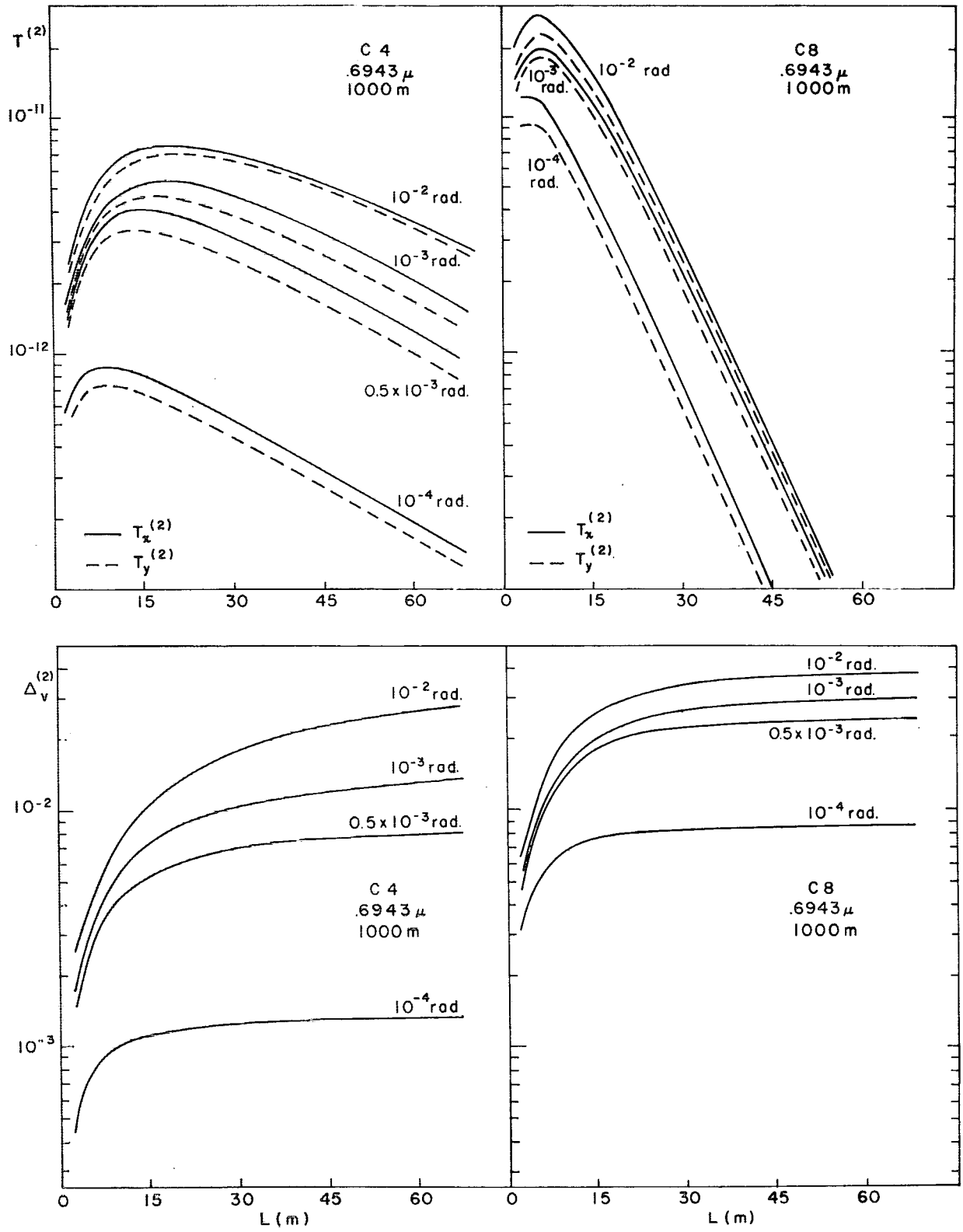

FIG. 11. The second-order power transfer functions (upper figures) and depolarization ratios (lower figures) for two cloud models, C4 and C8, with receiver beam widths of 10^{-2}, 10^{-3}, 0.5×10^{-3} and 10^{-4} rad. The particle number density is 100 cm^{-3}.

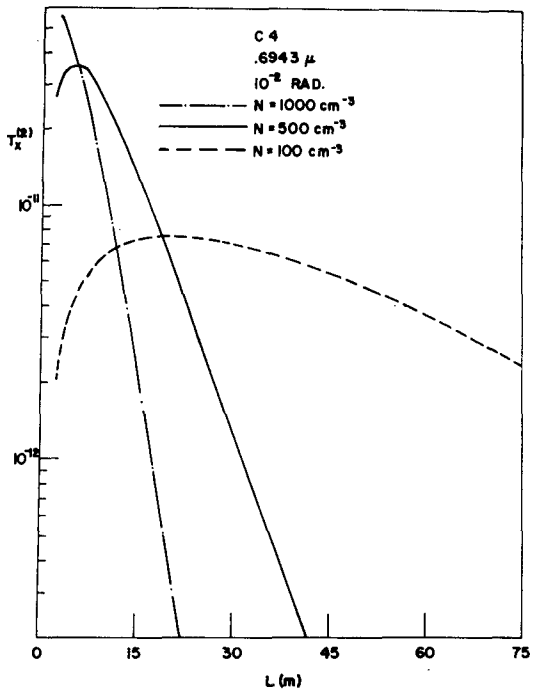

FIG. 12. Second-order power transfer functions (vertical component only) for different particle number densities of 100, 500 and 1000 cm^{-3}.

for beam widths varying from 10^{-2}–10^{-4} rad for a large particle size distribution such as occurs in stratiform clouds.

Thus, for a beam width on the order of 10^{-4} rad, the depolarization ratio is less than 1% in this calculation, and it may be neglected compared to, say, a 30% depolarization caused by backscattering from ice crystals (Schotland, 1969, unpublished laboratory results).

As shown by (2), two parameters contribute to the volume scattering cross sections β_s, namely, the mean scattering cross section and the particle number density. For homogeneously distributed cloud drops, $\beta_s = \bar{\sigma}_s N$. Thus, N plays a role equally as important as that of $\bar{\sigma}_s$. Physically, increasing β_s corresponds to either increasing the particle mean radius or the particle number density in the cloud. Since $\bar{\sigma}_s$ is determined by the cloud models, and since no significant difference in the phase functions for two size distributions is found, the values of the secondary backscattering and depolarization are mainly dependent on the values of the scattering cross section. In the previous calculations, the particle number density is assumed to be 100 cm^{-3}.

To get some idea of the effect of the particle number density on the calculations, we assume a cloud height of 1000 m and a beam width of 10^{-2} rad. It is found that the return power is very sensitive to the droplet number density. For larger N, it increases very rapidly to the peak power and then decreases very rapidly as a function of time (Fig. 12). The depolarization ratio for values of 100, 500 and 1000 cm^{-3} has been computed for C4 and C8 as shown in Fig. 13. The depolarization ratio increases with increasing particle number density for both size distributions. A difference of about 2% is calculated for a change in N from 500 to 100 cm^{-3} for C4, while less than 1% is seen for C8. No significant change of depolarization is found for drops of number density 500 and 1000 cm^{-3}. The reason is that the attenuation is so strong that the depolarization approaches a limiting value. About 4% depolarization is found for number densities of 500 and 1000 cm^{-3} in two cloud models.

As mentioned before, the volume scattering cross section is the product of the mean scattering cross section and the drop number density, so that the relationship of the two parameters is linear. Thus, since $\bar{\sigma}_s$ for C8 is about four times larger than that for C4 for wavelengths in the visible and near visible, we should expect the same values of the second-order transfer function and depolarization for C8 containing 100 particles cm^{-3} as for C4 containing 400 particles cm^{-3}. This argument was verified by our calculations.

The pulse length used in the above calculations is 3 m, which corresponds to a pulse duration of 10 nsec. The outgoing energy depends upon the pulse duration. According to the equations for the power transfer function, the backscattered flux densities received on the collecting aperture also depend on the pulse duration. Fig. 14 shows the second-order transfer function for two different pulse lengths of 3 and 1.5 m with other parameters constant. Since we can physically interpret a pulse length of 1.5 m as a 3 m pulse divided into two equal sub-pulses in the vertical direction, the received power from a pulse length of 3 m is the same as the sum of the received power from two pulse lengths of 1.5 m. However, the depolarization ratio does not depend upon the pulse length, because the value of the pulse length is cancelled out between the primary and secondary backscattering.

6. Conclusions

We have developed a method based on the geometry of a pulsed lidar system in which the total flux density of the secondary backscattered radiation for a polarized laser source is formulated from the radiative transfer relationships including the complete Stokes parameters for two orders of scattering. The power incident on the receiver can be computed by integrating over the perpendicular area of the collecting aperture. The depolarization ratio of the secondary backscattering from a volume of symmetrical and uniformly distributed water drops may therefore be defined.

It is shown in the separate paper by Liou (1971) that the value of the returned power from orders of scattering higher than the second is negligibly small compared to the secondary backscattering in the pulsed light system. Thus, the second-order power transfer function and depolarization may be used to "estimate" the total value of power transfer functions and depolarization due

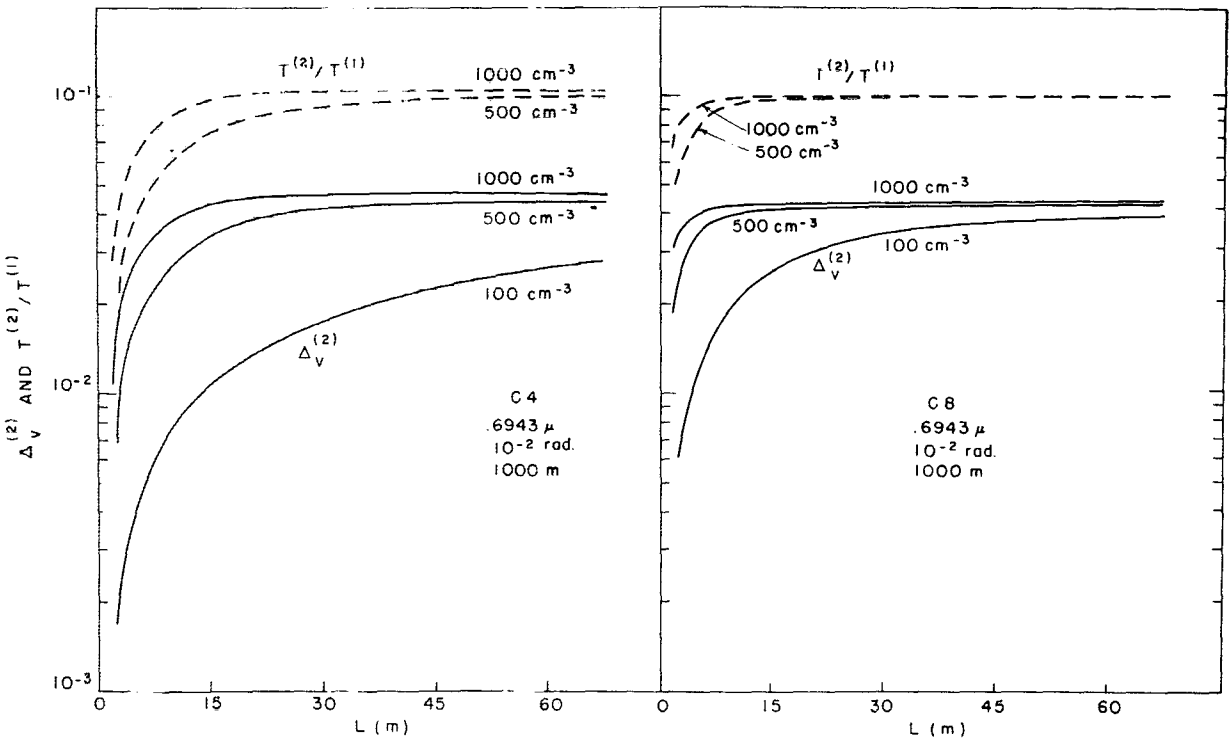

FIG. 13. The ratio of second- to first-order power transfer functions (dotted lines) and depolarization ratios (solid lines) of two cloud models, C4 (left) and C8 (right), for different particle number densities of 100, 500 and 1000 cm^{-3}.

to multiple backscattering from a linearly polarized laser source.

Variations in the returned power and depolarization are negligible for wavelengths in the visible and near visible from water clouds. This is verified by three typical laser wavelengths: 0.3472, 0.6943 and 1.06 μ. The return signals depend on the cloud height, and vary strongly with the clouds. A typical value of the returned power from the base of a cloud of 1000 m is about 90 db for the cloud model with mode radius at 4 μ, while that for a cloud model with mode radius at 8 μ is about 85 db. The returned power from the cloud base of 100 m is about 70 db for a cloud model with mode radius at 4 μ. Depolarization is not sensitive to the values of the cloud height. The drop number density within the cloud has a strong effect on the return signal. The depolarization ratio for different cloud particle densities is found to have maximum differences near the lower edge of the target. The depolarization and returned power are much larger for the cloud model with mode radius at 8 μ than for the model with mode radius at 4 μ. Since the return signal and depolarization strongly depend upon the beam width of the receiver, a beam width on the order of 10^{-4} rad is recommended in measuring the depolarization caused by multiple scattering. In this way, the difference between ice and water clouds may be distinguished by using the optical laser technique with backscattering.

According to the observations, the cloud contains well separated particles; that is, the average separation of the particles is much larger than the particle diameter, and the particles are not uniformly distributed. Thus, for incident wavelengths in the visible and near visible,

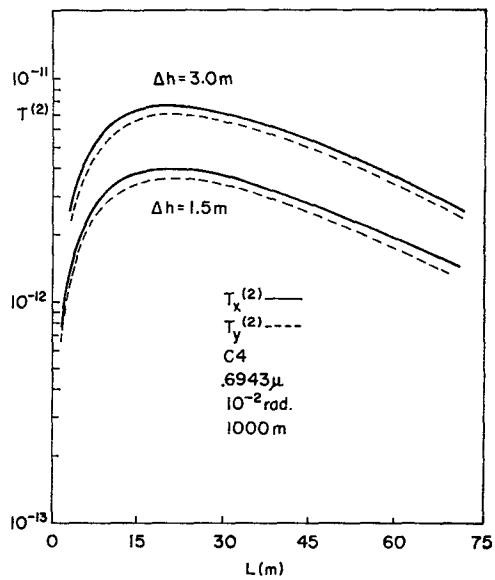

FIG. 14. Second-order power transfer function for two different pulse lengths of 1.5 and 3 m.

the assumption of independent scattering seems to be quite valid. However, the equation of radiative transfer does not include the effects of the particle motion which play an important role in the droplet growth process. Moreover, while cloud droplets are not homogeneously distributed in space, we have assumed a homogeneous cloud in our calculations in trying to take a first step in understanding the composition and structure of clouds. Therefore, it is possible to extend this work to study the effect on the depolarization of inhomogeneities in the cloud, and of particle motion within the cloud.

Finally, we believe that the calculations for the returned power from water clouds and the depolarization due to multiple scattering for a collimated pulsed lidar system are a fundamental study in this field. It is recommended that a measurement of multiple backscattering be made in the backscattered return from ground level or airborne laser radar, or possibly from satellites. From the depolarization or polarization measurements, more information on the composition and structure of the clouds should be obtained. The optical properties of the clouds may therefore be determined more accurately and more rigorously.

Similar types of calculations may be performed for ice clouds, although more parameters in the phase matrix will be involved due to non-sphericity of the particles. Furthermore, studies should be made of the effects of the shape and the index of refraction of ice crystals.

Acknowledgments. We would like to thank Dr. James Hansen for carefully reading a draft version of this paper. During the course of this research K. N. Liou held a National Research Council Postdoctoral Research Associateship supported by the National Aeronautics and Space Administration. We would also like to thank Dr. Robert Jastrow for his hospitality at the Institute for Space Studies.

REFERENCES

Atlas, D., M. Kerker and W. Hitschfield, 1953: Scattering and attenuation of non-spherical atmospheric particles. *J. Atmos. Terr. Phys.*, **3**, 108–119.

Battan, L. J., 1959: *Radar Meteorology*. The University of Chicago Press, 161 pp.

——, and C. H. Reitan, 1957: Droplet size measurement in convective clouds. *Artificial Stimulation of Rain*, London, Pergamon Press, 184 pp.

Bellman, R., H. Kagiwada and R. Kalaba, 1964: Invariant imbedding and time dependent transport processes—diffuse reflection with delta-function input. Memo. RM-4278-ARPA, The Rand Corporation, Santa Monica, Calif., 125 pp.

Borovikov, A. M., A. Khrgian *et al.*, 1961: *Cloud Physics*. Israel Program for Scientific Tranalation, 392 pp.

Chandrasekhar, S., 1960: *Radiative Transfer*. New York, Dover Publ., 393 pp.

Diermendjian, D., 1961: Mie scattering with complex index of refraction. *J. Opt. Soc. Amer.*, **51**, 620–633.

——, 1964: Scattering and polarization properties of water clouds and hazes in the visible and infrared. *Appl. Opt.*, **3**, 187–196.

——, 1969: *Electromagnetic Scattering on Spherical Polydispersions*. New York, Elsevier, 290 pp.

Dell-Imagine, R. A., 1965: A study of multiple scattering of optical radiation with application to laser communications. Tech. Rept., Dept. of Electrical Engineering, University of California at Los Angeles.

Diem, M., 1948: Messungen der Frosse von Wolkenelementen II. *Meteor. Rundschau*, **9**, 261–273.

Durbin, W. G., 1959: Droplet sampling in cumlus clouds. *Tellus*, **11**, 202–212.

Herman, B., 1965: Multiple scatter effects on the radar return from large hail. *J. Geophys. Res.*, **70**, 1215–1225.

Irvine, W. M., and J. B. Pollack, 1968: Infrared optical properties of water and ice spheres. *Icarus*, **8**, 324–366.

Liou, K. N., 1970: Calculations of multiple backscattered radiation and depolarization from water clouds for a collimated pulsed lidar system. Ph.D. thesis, Dept. of Meterorology and Oceanography, New York University, 78 pp.

——, 1971: Time-dependent multiple backscattering. *J. Atmos. Sci.*, **28**, 824–827.

Perrin, F., 1942: Polarization of light scattered by isotropic opalescent media. *J. Chem. Phys.*, **10**, 415–427.

Newell, R. E., S. Geotis and A. Fleischer, 1957: The shape of rain and snow at microwavelengths. Res. Rept. No. 28, Dept. of Meteorology, M.I.T.

Schotland, R. M., D. Chang and J. Bradley, 1965: Study of active probing of water vapor profiles and results of experiments. Final Rept. (Interim) GSL-TR-65-6, Dept. of Meteorology and Oceanography, New York University.

Singleton, F., and D. F. Smith, 1960: Some observations of drop size distributions in low layer clouds. *Quart. J. Roy. Meteor. Soc.*, **86**, 454–467.

Squires, P., 1957: The spatial variation of liquid water and droplet concentration in cumuli. *Tellus*, **10**, 373–380

van de Hulst, H. C., 1957: *Light Scattering by Small Particles* New York, Wiley, 470 pp.

Weickmann, H. K., and H. J. aufm Kampe, 1953: Physical properties of cumulus clous. *J. Meteor.*, **10**, 204–211.

Weinman, J. A., and K. Ueyoshi, 1969: The effect of the phase function at forward angles on light pulses scattered backward from a thin turbid medium. *J. Atmos. Sci.*, **26**, 600–603.